Chapter-5

Blank page

5. Taguchi's optimization of various parameters for tribological performance of polyalphaolefins-based nanolubricants using ball-on-disc tribometer

This chapter addresses the optimization of various control parameters by using Taguchi's method to assess the tribological properties of PAOs based nanolubricants. The experimentations were performed using "ball on disc" tribometer according to Taguchi's' L18 mixed orthogonal array. The analysis of variance (ANOVA) was adopted to estimate the most prominent factors influencing the tribological performance of nanolubricants. The various analytical tools were used to assess the probabilistic rationale for improvement in friction and wear properties.

5.1. Characterization of COOH-functionalized MWCNTs

The detailed structural and morphological characterizations of COOH-functionalized MWCNTs have been illustrated in the previous **Sections 4.1.1.**

5.2. Design of experiment by Taguchi's method

The appropriate use of the statistical tool is essential because it significantly affects the performance of the experiments and draws some reasonable conclusions. The design of the experiment and statistical analysis of experimental data are the two- fundamental interests. Effective experiments involve awareness about the main factors that affect the output. The design of the experiment (DOE) is a structured and systemized process for gathering and evaluating the vast volumes of data to achieve a complete evaluation of the factors being investigated [153]. It enables the statistical investigation of the impact of multiple input variables on the output or response of a process. Experiments can be planned using various approaches such as response surface methodology, factorial design, and Taguchi's techniques. In the present study, the Taguchi's method was used to examine the effect of

different input factors on the output parameters. Taguchi's method is a collection of mathematical and statistical strategies for a scientific probe to the inadequacy of traditional experimental methods and is also helpful for modelling and analysing the problems in which multiple variables affect the response of interest [154]. In the Taguchi's method, the experiment numbers were exceptionally decreased by the orthogonal array and minimized the effects of uncontrollable factors on the output parameters. The Taguchi's method employs a loss function to measure the fluctuation between the desired and experimental values. This loss function is further transformed into a signal-to-noise (S/N) ratio. The nomenclature signal and noise illustrate the favourable and unfavourable output characteristic values, respectively. The S/N ratio is the log function of the desired output and acts as the objective function for optimization, assist in data analysis and the forecast of the optimum results. In Taguchi's robust design [155], S/N ratio quality characteristics have been divided into three categories as "smaller the better", "larger the better" and "nominal the better". Since the goal of this investigation is to acquire the best tribological characteristics of nanolubricants. Therefore, the "smaller the better" type quality characteristic was opted and given in Eq. (5.1)

$$S/N = -10 \log \left[\frac{1}{n}\sum_{i=1}^{n} y_i^2\right] \tag{5.1}$$

Where, y_i is the quality characteristic at the i^{th} experiment, and n is the number of observations. Sliding velocity, applied load, the concentration of MWCNTs, and kinematic viscosity of PAOs were chosen as control parameters (or input factor), and their levels were decided as shown in **Table 5.1**. The coefficient of friction and specific wear rates were considered the response factors (or output parameters). An L_{18} mixed orthogonal array (i.e., three levels for three factors and six levels for one factor) was selected to evaluate and optimise response parameters. The designed experiments as per Taguchi's L_{18} orthogonal

array are illustrated in **Table 5.2**. All the statistical analysis involved in Taguchi's method was carried out by using minitab@18 software.

The calculations of film parameter (λ) have been done for all the experiments as explained in Appendix C, and corresponding values are shown in the respective columns in **Table 5.3**. PAO 4 and 6, were under unity for all experiments, which signifies that lubrication follows the boundary lubrication regime. However, in the case of PAO 40, the calculated values of λ vary greater than unity and less than unity, which is the potential evidence of a mixed to boundary lubrication regime.

Table 5.1: Experimental conditions (parameters and their levels)

Parameters	**Levels**					
	1	**2**	**3**	**4**	**5**	**6**
Concentration of MWCNTs (wt. %); A	0	0.025	0.050	0.075	0.10	0.15
Applied load (N); B	50	80	100			
Sliding velocity (m/s); C	0.420	1.099	1.570			
Kinematic viscosity ($\times 10^{-6}$; m^2/s); D	4	6	40			

5.3. Tribological performance of nanolubricants

5.3.1. Friction response of nanolubricants

5.3.1.1. Taguchi's optimization for COF

The COF was measured according to the orthogonal array (L_{18}) for all combinations of control factors via Taguchi's method. All measured values of COF were transformed into an S/N ratio with the help of the "smaller the better" condition. For minimum COF, the highest value of the S/N ratio is desirable for every factor because the highest value of the S/N ratio results in the lowest COF. The COF values and their corresponding S/N ratios are measured at different combinations of parameters, as shown in **Table 5.3**.

The average value of COF was estimated as 0.081, and the average S/N ratio value was found to be 22.52. The analysis of the effect of each input factor (A, B, C, D) on the COF was accomplished by a response table for the S/N ratio and presented in **Table 5.4**. This S/N ratio is also showcased in pictorial form in **Figure 5.1(a)**, demonstrating the optimal level (i.e., the highest S/N ratio) of control factors for COF. It is clear from **Figure 5.1(a)** and **Table 5.4** that the levels and S/N ratio for the factors offering the best COF were identified as factor A (Level 3, S/N=27.77), factor B (Level 3, S/N=24.25), factor C (Level 3, S/N=23.24), factor D (Level 2, S/N=23.78). In other words, the minimum COF value was attained at 0.05 wt.% concentration of MWCNTs (A_3), at an applied load (B_3) of 100 N, at sliding velocity (C_3) 1.57 m/s and with PAO 6 (D_2).

5.3.1.2. ANOVA analysis for COF

The analysis of variance (ANOVA) was performed to examine the factor that significantly affects the tribological characteristics. This analysis was conducted with a 5% significance level and at a confidence level of 95%. All ANOVA results are summarised in **Table 5.5**. The predominant input factors in ANOVA were decided by comparing the F value of all

input factors. The most significant control factor was identified through the highest F value among all factors, and the P-value should be less than 0.05. After meticulous probe of F and P value of all control factors (**Table 5.5**), it was observed that factor B (applied load) features the most significant influence on the COF, followed by factor A (concentration), factor D (kinematic viscosity) and factor C (sliding velocity). The last column of ANOVA analysis (**Table 5.5**) represents each factor's percentage contributions, which illustrates the degree of influence on COF. The percentage contribution of load (B), concentration (A), kinematic viscosity(D) and velocity (C) were found to be 47.1%, 39.3%, 6.6% and 3.7% respectively. The contribution of residual error was 2.2%.

Table 5.2: Matrix or designed experiments as per L_{18} orthogonal array

Experiment No.	**Factors**			
	A	**B**	**C**	**D**
1	1	1	1	1
2	1	2	2	2
3	1	3	3	3
4	2	1	1	2
5	2	2	2	3
6	2	3	3	1
7	3	1	2	1
8	3	2	3	2
9	3	3	1	3
10	4	1	3	3
11	4	2	1	1
12	4	3	2	2
13	5	1	2	3
14	5	2	3	1
15	5	3	1	2
16	6	1	3	2
17	6	2	1	3
18	6	3	2	1

Table 5.3: Experimental layout and obtained results

Exp. No.	Factors				COF (μ)	S/N ratio for μ (dB)	Specific wear rate (K; 10^{-8} mm^3/Nm)	S/N ratio for K, (dB)	Film thickness ratio (λ)
	A	B	C	D					
1	0	50	0.42	4	0.125	18.07	13.99	-22.92	0.058
2	0	80	1.099	6	0.060	24.44	5.51	-14.81	0.152
3	0	100	1.57	40	0.064	23.88	1.28	-2.17	1.098
4	0.025	50	0.42	6	0.108	19.34	5.35	-14.56	0.082
5	0.025	80	1.099	40	0.088	21.12	0.43	7.35	0.876
6	0.025	100	1.57	4	0.068	23.35	2.62	-8.37	0.136
7	0.05	50	1.099	4	0.083	21.65	4.42	-12.91	0.112
8	0.05	80	1.57	6	0.025	32.05	0.52	5.81	0.194
9	0.05	100	0.42	40	0.033	29.63	0.79	2.07	0.448
10	0.075	50	1.57	40	0.107	19.42	0.49	6.26	1.155
11	0.075	80	0.42	4	0.065	23.75	0.76	2.37	0.056
12	0.075	100	1.099	6	0.07	23.09	1.79	-5.07	0.150
13	0.1	50	1.099	40	0.114	18.85	1.01	-0.01	0.906
14	0.1	80	1.57	4	0.077	22.27	0.88	1.15	0.138
15	0.1	100	0.42	6	0.054	25.31	2.24	-7	0.078
16	0.15	50	1.57	6	0.119	18.49	3.17	-10.01	0.201
17	0.15	80	0.42	40	0.095	20.46	0.38	8.59	0.455
18	0.15	100	1.099	4	0.097	20.27	2.11	-6.46	0.107

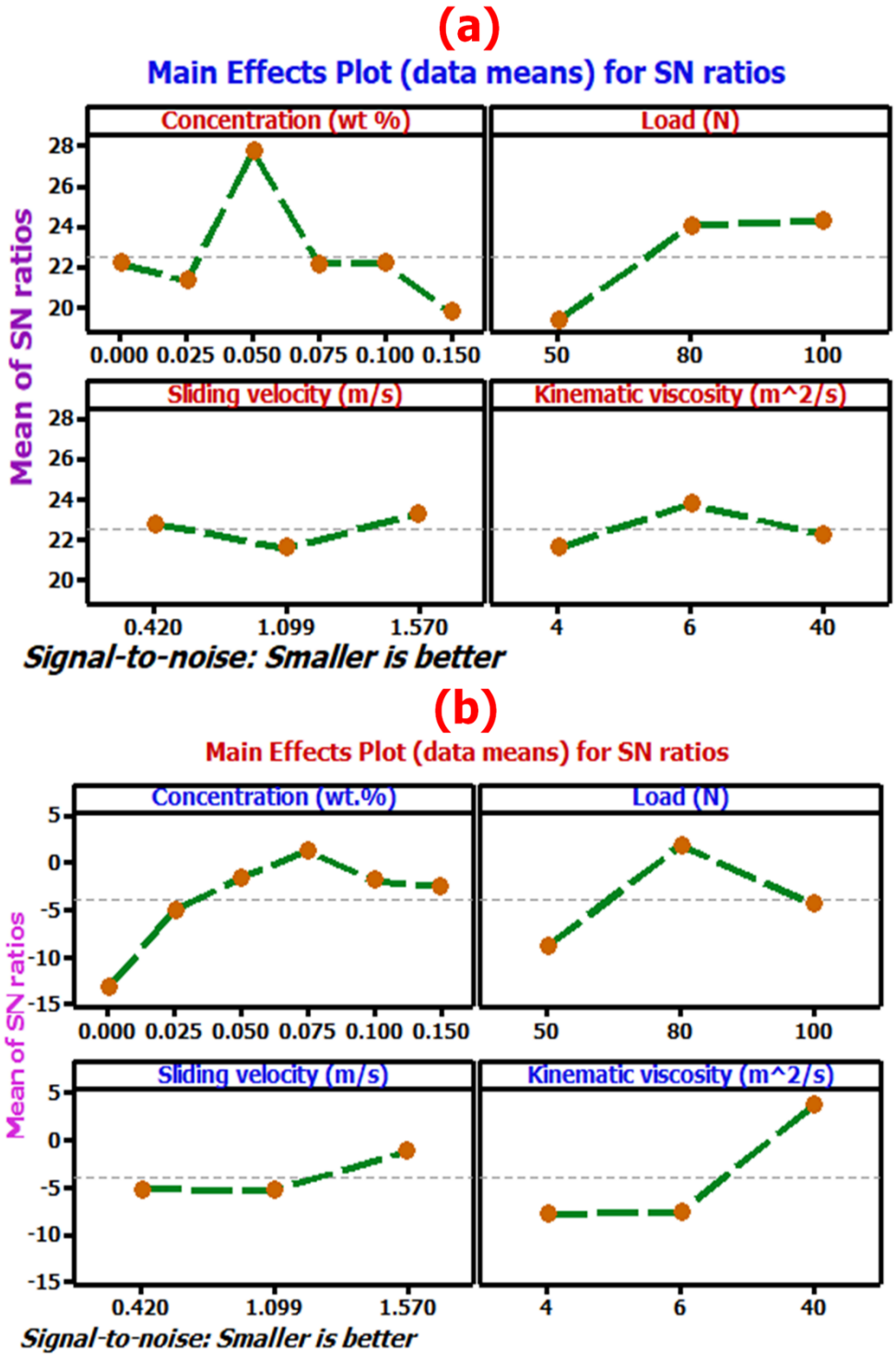

Figure 5.1: Influences of control parameter on S/N ratio for (a) COF, and (b) specific wear rate (K)

Table 5.4: Response table for S/N ratio for different parameters at different levels

Response	Parameter	Level					
		I	II	III	IV	V	VI
Mean COF	A	22.13	21.26	**27.77**	22.08	22.14	19.74
	B	19.3	24.01	**24.25**	-	-	-
	C	22.75	21.57	**23.24**	-	-	-
	D	21.55	**23.78**	22.22	-	-	-
Specific wear rate (K)	A	-13.3	-5.19	-1.67	**1.19**	-1.95	-2.63
	B	-9.1	**-1.75**	-4.5	-	-	-
	C	-5.24	-5.32	**-1.22**	-	-	-
	D	-7.86	-7.61	**3.68**	-	-	-

The predictive capability and the statistical accuracy of the model were examined by using R^2 value and shown in **Table 5.6**. The R^2 value is used to evaluate the effectiveness of the model. The developed model is adequate when the R^2 value is close to unity. The R^2 (0.966) and adjusted R^2 (0.903) of the COF elucidate that actual and predictive values of COF are very close proximate. All these determinations describe that the COF model can be further applied to examine the influences of factors on COF.

Figure **5.2(a)** displays the normal probability plot of COF. The normal probability plot is used to test the normality of experimental outcomes, and it reveals the predicted versus actual values for the design experiment layout. It is mandatory for ANOVA analysis that the normal probability plots should be tested for the spectrum of residuals located near to the mean line. Figure 5.2(a) shows that residual values are proximate to the mean line, specifying that the errors are normally distributed.

A multiple variable linear regression model was constructed using statistical software Minitab@18 to create the correlation between the input parameters (A, B, C, and D) and output response (COF). The generated regression equation, which is employed to predict the value of COF, is shown in Eq. (5.2).

$$Mean\ COF = 0.1435 + 0.141A - 0.000936B - 0.0022C + 0.000105D \quad (5.2)$$

Where A is the concentration of MWCNTs (wt.%), B is applied load (N), C is sliding velocity (m/s), and D is kinematic viscosity (m^2/s).

5.3.1.3. Effect of control factor on COF

The average COF values of control factors at different levels are given in Table 5.7. For factor A (i.e., the concentration of MWCNTs), COF varies from 0.083 to 0.104. The minimum COF (0.047) was obtained at an optimum concentration of 0.05 wt.%. However, it was also noticed that further increasing the dose of additive beyond the optimum level leads to an increase in COF. At an optimum concentration, MWCNTs can easily get deposited into the grooves and valleys of rubbing surfaces and provide an effective rolling and mending effect. Therefore, COF has decreased significantly. Although the presence of higher concentrations of the additive may develop a large cluster due to aggregation of nanotubes which may diminish the rolling effect, consequently, it may cause ploughing action on the base metal due to hard and brittle nature MWCNTs and introduces higher COF [133].

Table 5.5: Analysis of variance (ANOVA) for coefficient of friction (COF; μ) and specific wear rate (K)

Source	DF		Seq SS		Adj MS		F-value		P-value		Contribution (%)	
	μ	K	μ	K	μ	K	μ	K	μ	K	μ	K
Concentration (wt. %)	5	5	93.65	378.97	22.43	175.45	16.47	32.56	0.002	0.001	39.3	28.1
Applied load (N)	2	2	112.15	350.90	46.83	75.79	34.38	14.07	0.001	0.003	47.1	26.0
Sliding velocity (m/s)	2	2	8.89	65.93	4.45	32.97	3.26	6.12	0.110	0.036	3.7	4.9
Kinematic viscosity ($\times 10^{-6}$; m^2/s)	2	2	15.69	521.40	7.84	260.70	5.76	48.39	0.040	0.000	6.6	38.6
Residual Error	6	6	5.14	32.33	1.36	5.39					2.2	2.4
Total	17	17	238.55	1349.53								

DF- **Degree of freedom,** μ-**Coefficient of friction (COF),** K-**Specific wear rate**, Seq SS- **Sequential sum of squares,** Adj MS- **Adjusted mean squares**

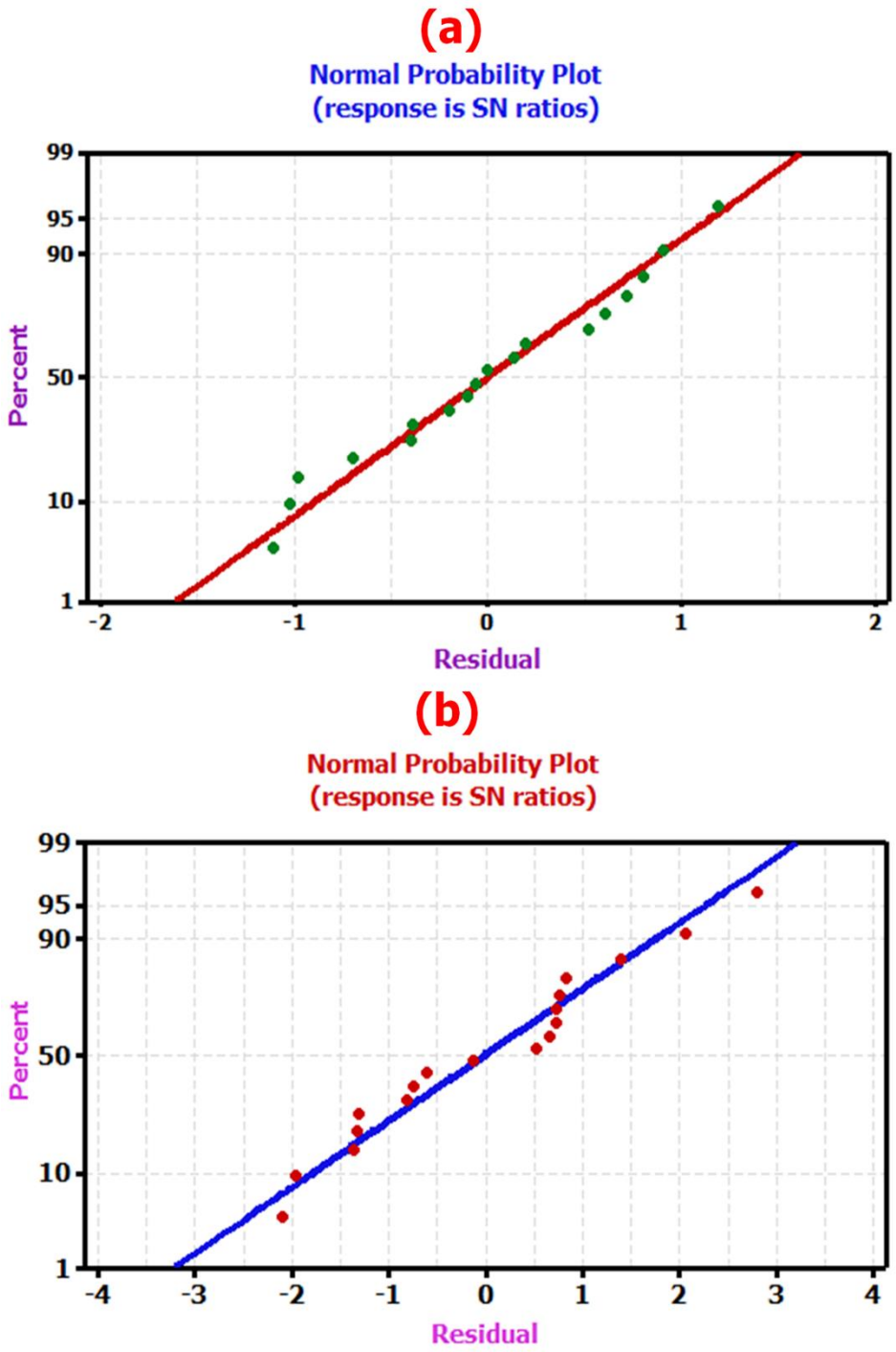

Figure 5.2: Normal probability plot for (a) COF, and (b) specific wear rate (K)

Table 5.6: The summary of model for responses

	COF (μ)	Specific wear rate (K)
R	0.982	0.986
R-squared (%)	0.966	0.976
Adjusted R-squared (%)	0.903	0.932

It is apparent from **Table 5.7** that COF was inverse to factor B (applied load). In other words, as the applied load increases, the decreasing trend of COF was identified. The minimum COF was ascertained at a load of 100 N. Due to an increase in the applied load, and few MWCNTs may be deformed in lamella form and lie flat at the interface during the friction process and produce a low energy surface leading to lowering the COF. In other words, generally, lubricants are assumed to be squeezed out under a higher applied load. In such a case, MWCNTs acts as an effective intermediator (i.e., solid lubricant), restricting the contact of friction pairs [62].

Factor C (sliding velocity) showed a similar trend to factor B. Increase in the sliding velocity from 0.42 to 1.57 m/s, the COF continuously decreased. This reduction in COF is due to high surface contact temperature induced by the dynamic collision of the asperities of the steel surface, MWCNTs, and base oil at a higher velocity resulting in the formation of impermeable tribo-layer (protective layer) by in situ tribo-chemical reactions. Therefore, this might have protected the friction surfaces and reduced the COF.

The factor D (kinematic viscosity) did not significantly influence COF compared to other factors, as shown in the ANOVA **Table 5.5**. The COF has continuously decreased as kinematic viscosity increases from 4×10^{-6} m^2/s to 6×10^{-6} m^2/s and then increases up to 40×10^{-6} m^2/s. The minimum COF was obtained at a kinematic viscosity of 6×10^{-6} m^2/s (i.e., PAO 6). The results indicate that higher viscous lubricant (PAO 40) could not considerably

affect COF compared to PAO 6. However, it has exhibited better frictional characteristics as compared to PAO 4. The possible reason is that when the kinematic viscosities of PAOs increases, the minimum film thickness also increases (calculated from **Eq. C.1 of Appendix C**). The shearing action of lubricants will become rigorous with an increase in the kinematic viscosity of the oil. More energy is expected to deal with this state. Consequently, it increases the COF.

The contour plots shown in **Figure 5.3**, constructed with Minitab@18 software to know the effect of the interaction of these factors on the COF. The contour plot is a graphical portrayal representing the relationship between the three numeric variables in two dimensions. It is evident from the ANOVA **Table 5.5** that the applied load and concentration of MWCNTs are the most influential factor, and their combined effect on COF are displayed in **Figure 5.3(a)**. The range of COF values for a particular colour is shown in the dialogue box of the respective contour plot. The minimum values of COF were predicted at 0.05 wt.% of MWCNTs and in the vicinity of 70 to 100 N (indicated by light blue colour). If a point is fixed at 0.05 wt.% concentration, then COF linearly decreases with increasing the load from 50 to 100 N. However, the concentration reveals the non-monotonic effect on COF when the point is fixed at 100 N load. Within the selected concentration range (0-0.15 wt.%), the COF is reduced to optimum value and increased with the further inclusion of MWCNTs. The above results of the contour plot (**Figure 5.3(a)**) are illustrated in **Figure 5.1(a)** and **Table 5.7**. The contour plots have also revealed the influences of the interaction of other factors, as depicted in **Figures 5.3(b)-5.3(f)**.

Table 5.7: Mean response table for COF and K for various parameters at different levels (Note: Bold values shows the optimal levels of control factors)

Response	Parameter	Level					
		I	II	III	IV	V	VI
Mean COF	A	0.083	0.088	**0.047**	0.081	0.082	0.104
	B	0.110	0.068	**0.064**	-	-	-
	C	0.080	0.085	**0.077**	-	-	-
	D	0.086	**0.077**	0.084	-	-	-
Specific wear rate (K; 10^{-8} mm^3/Nm)	A	6.9	2.8	1.9	**1.1**	1.4	1.9
	B	4.7	**1.4**	1.8	-	-	-
	C	3.9	2.5	**1.5**	-	-	-
	D	4.1	3.1	**0.7**	-	-	-

The friction behaviour of PAOs investigated at different operating conditions is opted from the experimental layout (**Table 5.3**). The selection of operating conditions is based on pure PAOs and PAOs containing MWCNTs showing the minimum value of COF. **Figure 5.4** shows the variation in COF with sliding distance for different operating conditions. Generally, two types of friction regimes are reported in the literature, i.e., running in period and steady-state period. **Figure 5.4(a)** illustrates the friction behaviour of pure PAO 4 tested at a sliding velocity of 0.42 m/s and a load of 50 N. It can be noticed that variation in COF indicates the trend of gradual increase then decrease and again increase followed by fluctuation till the end of the test. The obtained mean COF was 0.125 and is given in **Table 5.3** (experiment no.1).

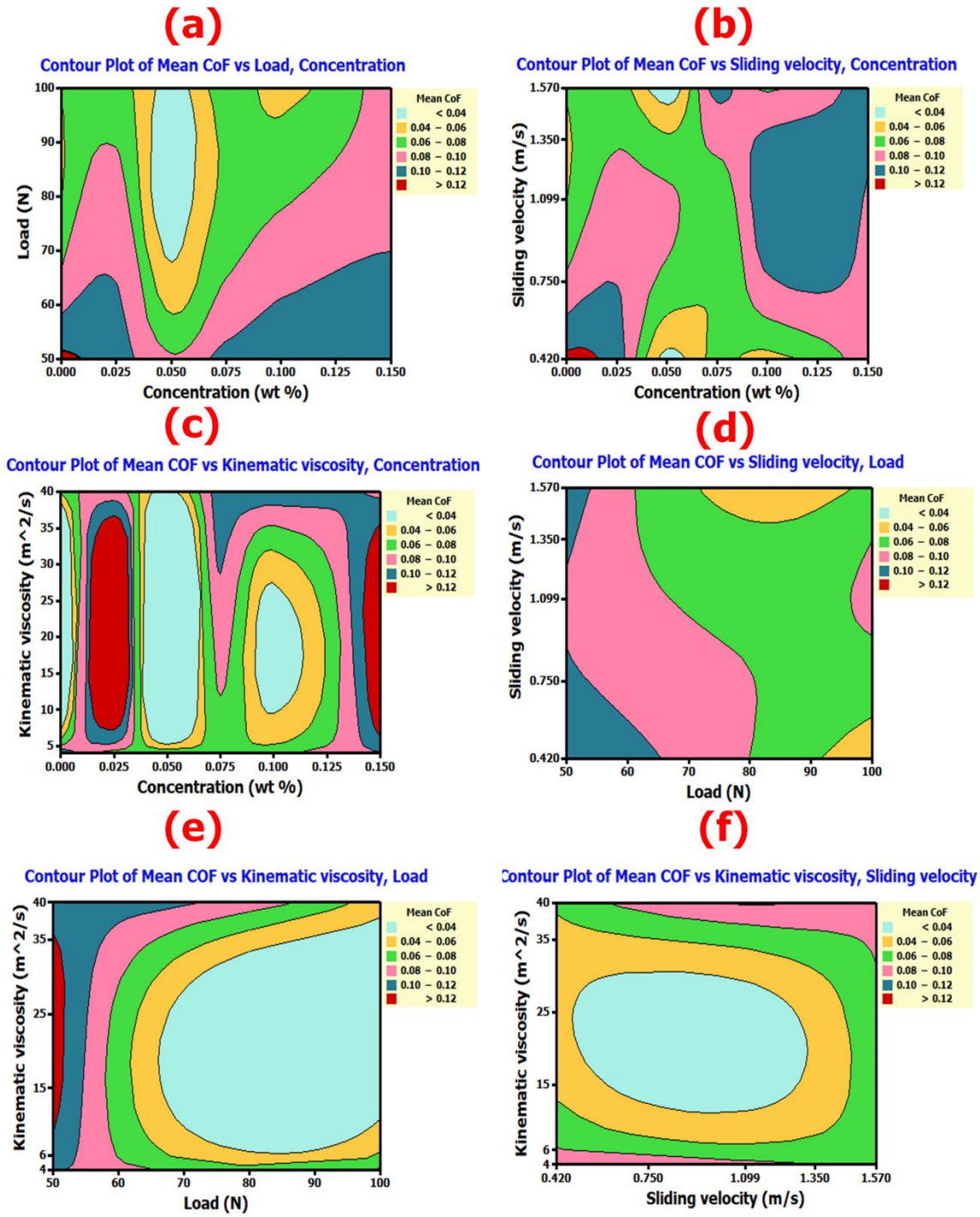

Figure 5.3: Contour plot demonstrates the effect of interactions of control factors on COF

In the case of PAO 4, the minimum COF was acquired with 0.075 wt.% of MWCNTs and tested at a sliding velocity of 0.42 m/s and a load of 80 N as shown in **Figure 5.4(b)** and **Table 5.3** (i.e., experiment no.11). **Figures 5.4(a)** and **5.4(b)** implies that the kinematic

viscosity and sliding velocity are the same in an opted test condition for PAO 4. Hence, the concentration of additive and load play a vital role in reducing the COF. The COF was decreased from 0.125 to 0.064 and exhibited a reduction of approximately 48 %. The thickness ratio (λ) also reduced from 0.058 to 0.056, which may be due to applying a higher load (80 N). The variations of COF of PAO 6 at different test conditions are displayed in **Figures 5.4(c)** and **5.4(d)**. The test conditions for pure PAO 6 and with optimum additive concentration and corresponding COF values are given in **Table 5.3** (i.e., experiment no. 2 and 8, respectively). It can be observed from **Table 5.3** that the applied load is the same for both test condition while sliding velocity increase from 1.099 to 1.57 m/s. The fluctuations in COF, shown in **Figure 5.4(d)**, are less than **Figure 5.4(c)**. The results illustrate that there is no steady-state period in COF. Furthermore, the COF has been reduced with an increase in sliding distance. This can be accomplished by the combined effect of optimum concentration of additive and higher sliding velocity, resulting in an increased thickness ratio (λ) from 0.154 to 0.194. Therefore, this might have helped in reducing the COF. In the case of PAO 40 (**Figures 5.4(e)** and **5.4(f)**), the decrease in COF may be attributed when lowering the sliding velocity from 1.57 to 0.42 m/s and addition of 0.05 wt.% of MWCNTs in PAO 40. The lubrication regime changes from mixed (λ=1.098) to boundary (λ=0.448) lubrication. PAO 40 is a highly viscous lubricant among all the lubricants tested in this study, causing more friction and energy loss (**Table 5.3**, experiment no. 3). PAO 40 with 0.05 wt.% MWCNTs demonstrated the minimum COF at sliding velocity of 0.42 m/s (**Table 5.3**, experiment no. 9), which may be ascribed to the rolling motion of MWCNTs under low sliding velocity and higher applied load, resulting in the formation of the low energy surface. The effect of all tested conditions on COF is more comprehensible through the contour plot (**Figure 5.3**).

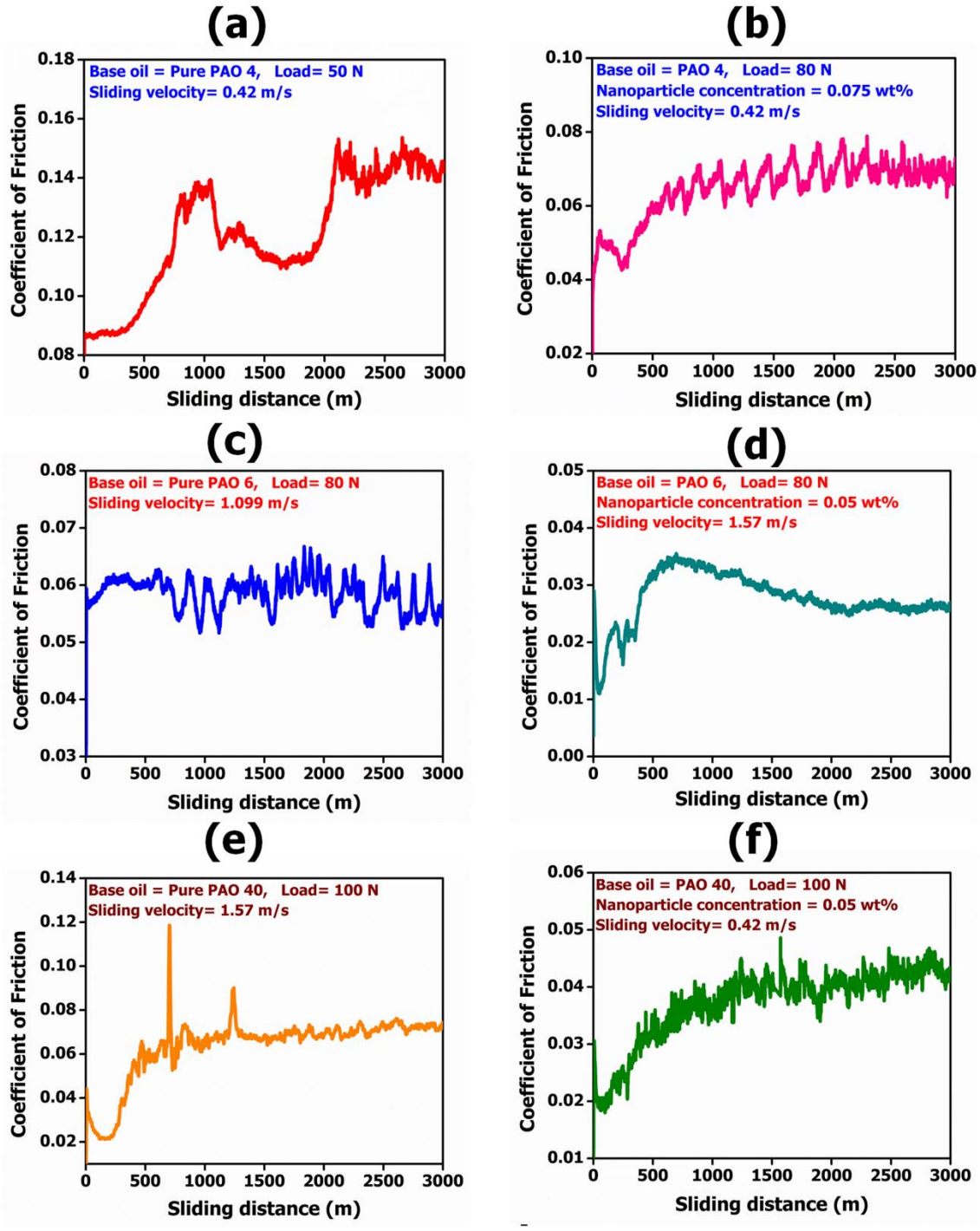

Figure 5.4: Variation in COF as a function of sliding distance for different operating conditions

5.3.2. Wear response of nanolubricants

5.3.2.1. Taguchi's optimization and ANOVA analysis for specific wear rate (K)

Taguchi's optimization and ANOVA analysis of specific wear rate (K) were similar to the COF evaluation (**section 5.3.1.1** and **section 5.3.1.2**). It can be observed from **Table 5.4** and **Figure 5.1(b)** that the optimum setting of control factor that yields minimal K was found to be as factor A at level 4, factor B at level 2, factor C at level 3, and factor D at level 3. In other words, the minimum K was acquired with the introduction of 0.075 wt.% of MWCNTs in PAO 40 at an applied load of 80 N and sliding velocity of 1.57 m/s.

The ANOVA analysis for specific wear rate (K) is tabulated in **Table 5.5**, and this correlates various control factors, F and P values, and the % contribution of input factors. An interesting prediction is the dominance of kinematic viscosity of the lubricant, followed by the concentration of nanoadditive and the applied load on the K with a percentage contribution of 38.9 %, 28.1%, and 26 %, respectively. The ANOVA table (**Table 5.5**) also illustrates that sliding velocity is not a significant control factor within the selected range of confidence level. The R^2 and predicted R^2 value of the generated model for the K are ascertained to be 0.976 and 0.932, respectively, and it is given in **Table 5.6**, which are very close to each other and validating the good predictability of the developed model within the spectrum of control factors being studied. It can also be identified from **Table 5.6** that the developed model for K is more significant as compared to the COF model due to higher R^2 values. The regression equation obtained from a model of K and evaluated for their normality (**Figure 5.2(b)**) is presented in Eq. (5.2).

$$Mean\ specific\ wear\ rate\ (K) = 12.84 - 27.4A - 0.063B - 2.1C - 0.084D \qquad (5.3)$$

Where specific wear rate (K) in (mm^3/Nm), A is the concentration of MWCNTs (wt.%), B is applied load (N), C is sliding velocity (m/s), and D is kinematic viscosity (m^2/s).

5.3.2.2. Effect of control factors on specific wear rate (K)

The influence of the interaction of various input variables on K is represented in the contour plot (**Figure 5.5**), and **Table 5.7** demonstrates the mean K of different control factors at different levels. The results indicated that kinematic viscosity (factor D) played a crucial role in diminishing the K of steel balls. A significant decrease in the K of steel ball was noticed when kinematic viscosity increased from 4×10^{-6} to 40×10^{-6} m^2/s (Table 5.7). At higher kinematic viscosity (i.e., PAO 40), the mixed lubrication effect ($\lambda>1$) has caused the separation of friction pairs and resulted in decreasing the wear. The PAO 40 revealed the least K (0.7×10^{-8} mm^3/Nm) among all factors and exhibited the reduction in K of approximately 83% and 77% compared to PAO 4 and PAO 6, respectively. With the increase in the concentration of MWCNTs (factor A), a decreasing trend of K prevailed up to the optimum concentration, and thereafter, K increases with an increase in the concentration of additive. It was estimated from the results that a superior impact on wear resistance might be acquired as the concentration of additive was 0.075 wt.%. In the case of applied load (factor B), the K decreases from 4.7×10^{-8} to 1.4×10^{-8} mm^3/Nm as the load increases from 50 to 80 N. Afterwards, K displayed a mild increasing trend, i.e., K increased from 1.4×10^{-8} to 1.8×10^{-8} mm^3/Nm, when the load increased from 80 to 100 N. It was speculated that the lubricant film developed at the interfaces might be easily removed at a higher load (100 N). Therefore, material removal was increased, resulting in a higher K [83]. Furthermore, for sliding velocity (factor C), the K trend consistently declines with the sliding velocity. The identical behaviour was also observed for mean COF. At higher sliding velocity, there is a short interval of time for the individual asperities to come in

contact, thus less time for the asperities to deform and consequently reduction in wear and COF.

5.3.3. Confirmation test

The confirmation test is the last stage of the optimization process, recommended in Taguchi's method. It is mandatory to validate the results obtained from the Taguchi optimization approach. The confirmation tests were conducted at the optimum level of control factors, and measured values of COF and K are shown in **Table 5.8**. It was reported that the error should be lower than 20 % [156]. The calculated percentage error for COF and specific wear are 13.6 % and 18.8 %, respectively, and lie within the acceptable range. Therefore, these errors satisfactorily verified the robustness of the developed model at a 95% confidence level in the spectrum of experimental operating conditions and exhibited a good agreement between the predicted and confirmation test results.

Table 5.8: The summary of comparisons of predicted and confirmation test results

Response	Optimum testing condition	Predicted	Experimental	% Error
Coefficient of friction (COF)	A_3 B_3 C_3 D_2	0.019	0.022	13.6
Specific wear rate (K) ($\times 10^{-8}$ mm^3/Nm)	A_4 B_2 C_3 D_3	0.056	0.069	18.8

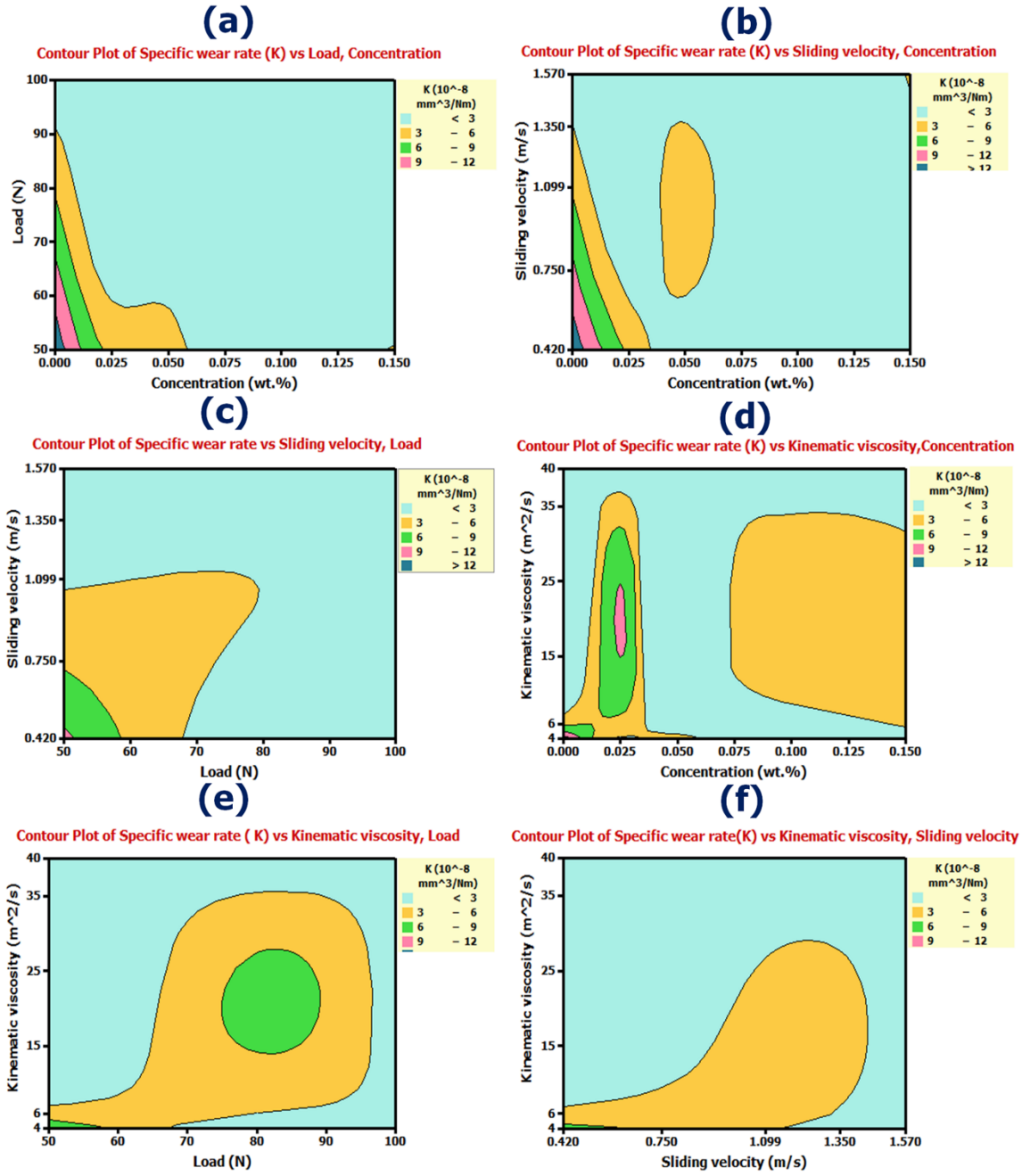

Figure 5.5: Illustrates the contour plot to show the influence of interactions of control factors on the specific wear rate (K)

5.4. Dispersion stability analysis of nanolubricants

The discussion in the preceding sections has affirmed the efficacy of MWCNTs as an additive in PAO oils for improving the tribological properties. To recommend their use in long-term applications, the lubricants should be tested for dispersion stability of MWCNTs in PAO oils. The sedimentation method is the easiest method to probe the dispersion

stability of nanolubricants. The tribological performance of nanolubricants depends on the velocity of nanoparticles at which they settle down on the base. The dispersion stability is a function of nanoparticle size, which controls the sedimentation velocity of nanoparticles in an oil medium [68]. Nanoparticles may attain low or high sedimentation velocities depending on particle size and lubricant viscosity. In the beginning, nanoparticles acquire random distribution as a result of the Brownian motion. A while later, the nanoparticles attain equilibrium in the oil. This transforms the random distribution of nanoparticles into ordered distribution, and the nanoparticles achieve a constant sedimentation velocity at the steady-state. The sedimentation velocity can be determined as per Stoke's law [157] as given in Eq. (5.4).

$$V_s = \frac{gd^2}{18\eta_0}(\rho_M - \rho_L) \tag{5.4}$$

Where V_s is the sedimentation velocity, g is the gravitational acceleration (m/s^2), d is the outer diameter of MWCNTs (m), η_0 is the dynamic viscosity of lubricant (PaS), ρ_M and ρ_L are the density of MWCNTs and lubricant (kg/m^3), respectively.

The calculated sedimentation velocities for PAO 4, PAO 6, and PAO 40 was 6.7×10^{-3}, 4.1×10^{-3} and 2.9×10^{-4} nm/s respectively. The lowest sedimentation velocity was found in PAO 40 base nanolubricant, implying that MWCNTs will take more time to settle down at the bottom. Accordingly, anti-wear performance was superior compared to other tested nanolubricants (**Table 5.3**). In contrast, due to the lowest dynamic viscosity among all the base oils, PAO 4 based nanolubricants obtained the highest sedimentation velocity.

The sedimentation of MWCNTs in all tested nanolubricants was analysed at room temperature (~ 30 °C) visually via photography method over a period of time, as shown in **Figure 5.6**. After 24 hours, MWCNTs concentrations, i.e., 0.025-0.075 wt.% in PAO 4 and

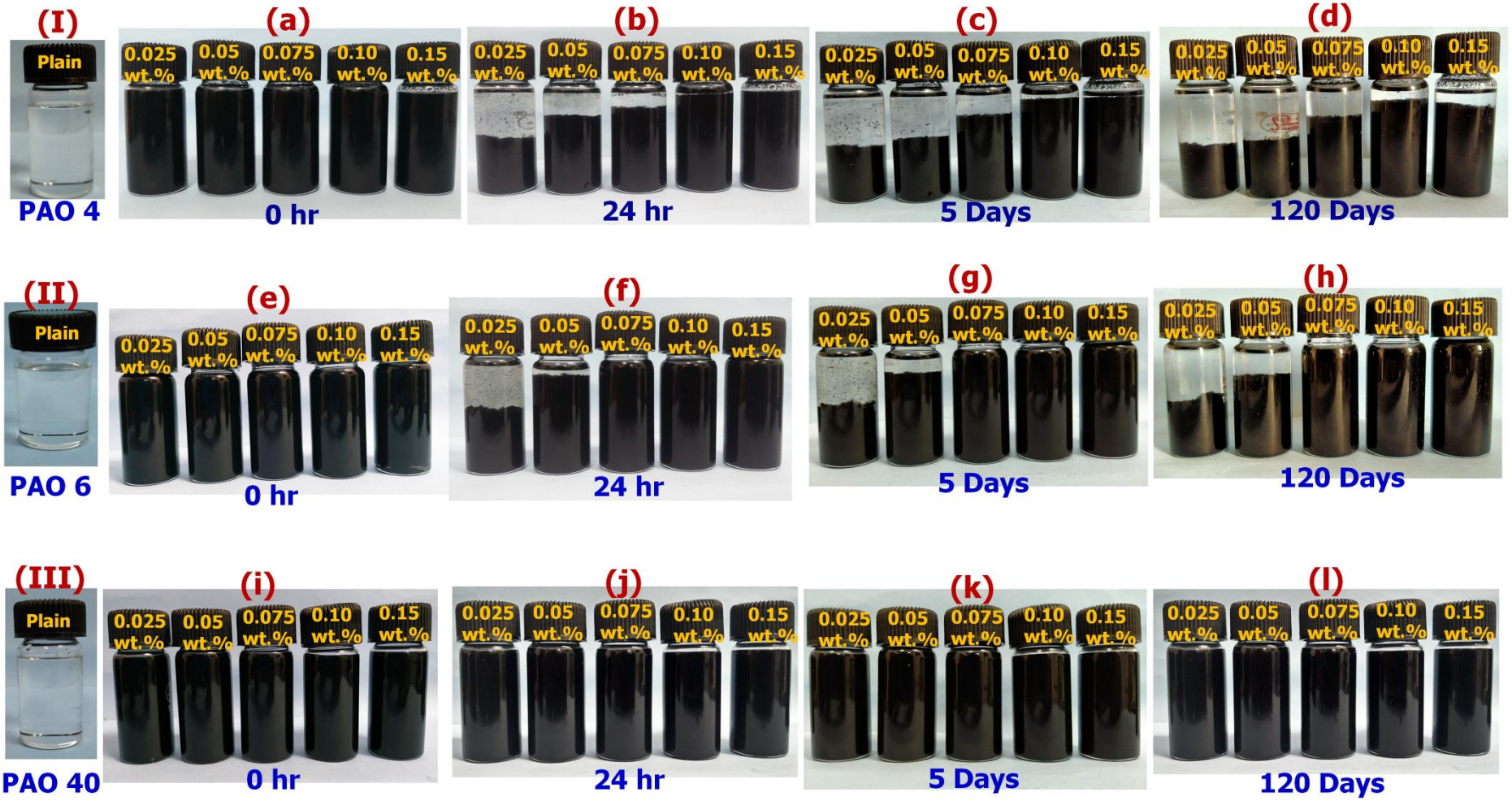

Figure 5.6: The photograph represents the dispersion stability of MWCNTs at room temperature (~ 30 °C) in different PAOs at different time interval

The sedimentation of MWCNTs in all tested nanolubricants was analysed at room temperature (~ 30 °C) visually via photography method over a period of time, as shown in Figure 5.6. After 24 hours, MWCNTs concentrations, i.e., 0.025-0.075 wt.% in PAO 4 and 0.025-0.05 wt.% in PAO 6 have begun to precipitate at the bottom of oils, and this phenomenon of sedimentation was observed up to 120 days. In contrast, no evidence of sedimentation was observed at 0.075-0.15 wt.% of MWCNTs in PAO 6 (**Figures 5.6(e)-5.6(h)**) and all dose of additive in PAO 40 (**Figures 5.6(i)-5.6(l)**) even after 120 days. The role of the functional group and in-situ suspension mechanism of MWCNTs in PAOs is described in **Figure 5.7**. The functional groups are organic compounds that consist of a polar head (hydrophilic) and non-polar tails (hydrophobic). The hydrophilic head linked to the surface of MWCNTs and hydrophobic tail encounter with PAO oil, which alter the surface energy of MWCNTs. Therefore, the dispersion stability of the MWCNTs in PAO oils is enhanced for an extended period.

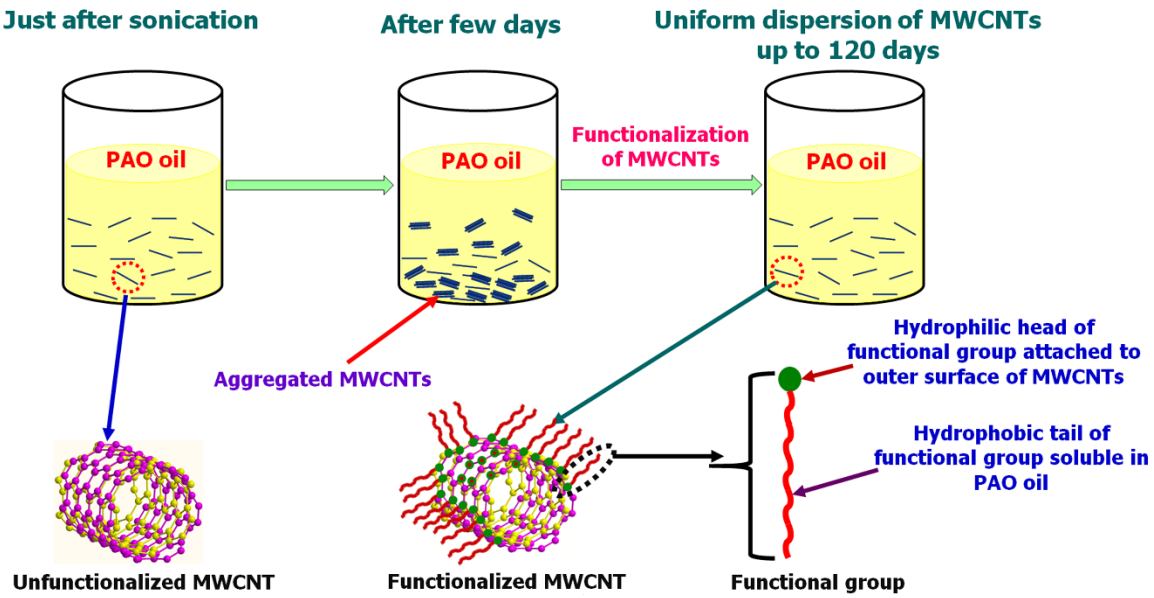

Figure 5.7: Illustrates the contribution of the functional group in the enhancement of suspension stability of MWCNTs in PAO oils

5.5. Study on morphology and topography of worn surfaces

Figure 5.8 displays the SEM of worn surfaces of steel balls tested under different experimental conditions. **Figures 5.8(a)-5.8(a_1)** correspond to the worn surface of the steel ball tested with pure PAO 4 at a sliding velocity of 0.42 m/s and 50 N load (experiment no. 1 of Table 5.3). Micrographs revealed a larger wear scar with wide, deep furrows and a large amount of wear debris, and this is a possible sign of abrasive and adhesive wear and plastic deformation of worn surfaces. As there were no additives in PAO 4, the lubricant film developed between the mating pair was very thin (λ=0.056), which was not sustained under the applied load of 50 N (Hertzian stress ~ 1.7 GPa) with continuous sliding. Consequently, direct metal-to-metal contact led to high wear. In contrast, worn surface of steel ball tested with PAO 4 containing 0.075 wt.% of MWCNTs at sliding velocity of 0.42 m/s and a load of 80 N (experiment no. 11 of Table 5.3) exhibited the lower wear scar with narrow furrow. **Figures 5.8(b)-5.8(b_1)** illustrate mild abrasive wear on the friction surfaces. As discussed earlier, under higher load (80 N), MWCNTs developed a thin lubricant film that has covered the surface asperities and developed relatively sleek surfaces. The MWCNTs in contact with mating surfaces may slip and slide and establish a shield that can be sustained under high frictional forces. This demonstrates the combined presence of abrasive grooves and polished smooth surfaces of the wear scar produced by the PAO 4 containing 0.075 % MWCNTs. **Figures 5.8(c)-5.8(c_1)** indicate micrographs of worn surfaces tested with pure PAO 6 at a sliding velocity of 1.099 m/s and a load of 80 N (experiment no. 2 of Table 5.3). While **Figures 5.8(d)-5.8(d_1)** indicate micrographs of worn surfaces tested with PAO 6 comprising of 0.05 wt.% of MWCNTs at a sliding velocity of 1.57 m/s and a load of 80 N (experiment no. 8 of Table 5.3). The results indicate that the existence of MWCNTs in PAO 6 has declined the magnitude of wear scar (**Figure 5.8(d)-5.8(d_1)**). The smallest wear scar and smoothest surface with light furrow along the sliding

direction were obtained when the surfaces were lubricated with PAO 40 containing 0.075 wt.% MWCNTs and tested at a sliding velocity of 1.57 m/s and a load of 50 N, as shown in **Figures 5.8(f)-5.8(f_1)**. The highly viscous characteristic of PAO 40 assisted in forming the mixed lubrication regime (λ= 1.16). This resulted in the separation of the mating surfaces and enhanced anti-wear performance. The wear-resistant property of PAO 40 was further improved with the addition of an optimum dose of MWCNTs (0.075wt.%), as shown in **Figures 5.8(f)-5.8(f_1)**.

The topographic images of 2D and 3D view and corresponding roughness values of worn surfaces of steel balls for different operating conditions are shown in **Figure 5.9** and **Table 5.9**. **Figures 5.9(a)-5.9(a_1)** indicate the topographic images of pure PAO 4 (experiment no.1), revealing the ploughing marks and deeply grooved features on the worn surface, signifying the severity of wear (as shown in **Table 5.3**). The average area roughness (S_q) was found to be 284.9 nm. The incorporation of 0.075 wt. % MWCNTs in PAO 4 (**Figures 5.9(b)-5.9(b_1)**) showed less furrows along with a smooth surface and abated the average area roughness (S_q) to 16.8 nm. The average area roughness (S_q) of the worn surface lubricated by pure PAO 6 (**Figures 5.9(c)-5.9(c_1)**) was ascertained to be 17.9 nm. The topographic image (**Figures 5.9(d)-5.9(d_1)**) demonstrated the deep scratch appearance of the worn surface when 0.05 wt.% MWCNTs was doped into PAO 6, which worsened the roughness compared to pure PAO 6. The average area of roughness (S_q) is increased by approximately 56%. It was reported that at higher loading conditions, the MWCNTs might break in the form of small fragments, which may adhere to the friction surface and improve the wear resistance and COF (**Table 5.3** and **Figure 5.4**). On the contrary, the adhesion of fragments may affect the characteristics of worn surfaces in terms of either degrade or comparably enhance [158]. In this study, the worn surface lubricated by PAO 6 incorporating 0.05wt% of MWCNTs was relatively bumpy in comparison to the worn

surfaces tested with pure PAO 6 **(Figures 5.9(d)-5.9(d_1))**. The SPM results elucidated that the worn surface tested with PAO 40 containing 0.075 wt.% MWCNTs (**Figures 5.9(f)-5.9(f_1)**) revealed the minimum roughness of 12.5 nm among all the tested conditions, which are also justified by SEM results (**Figure 5.8**).

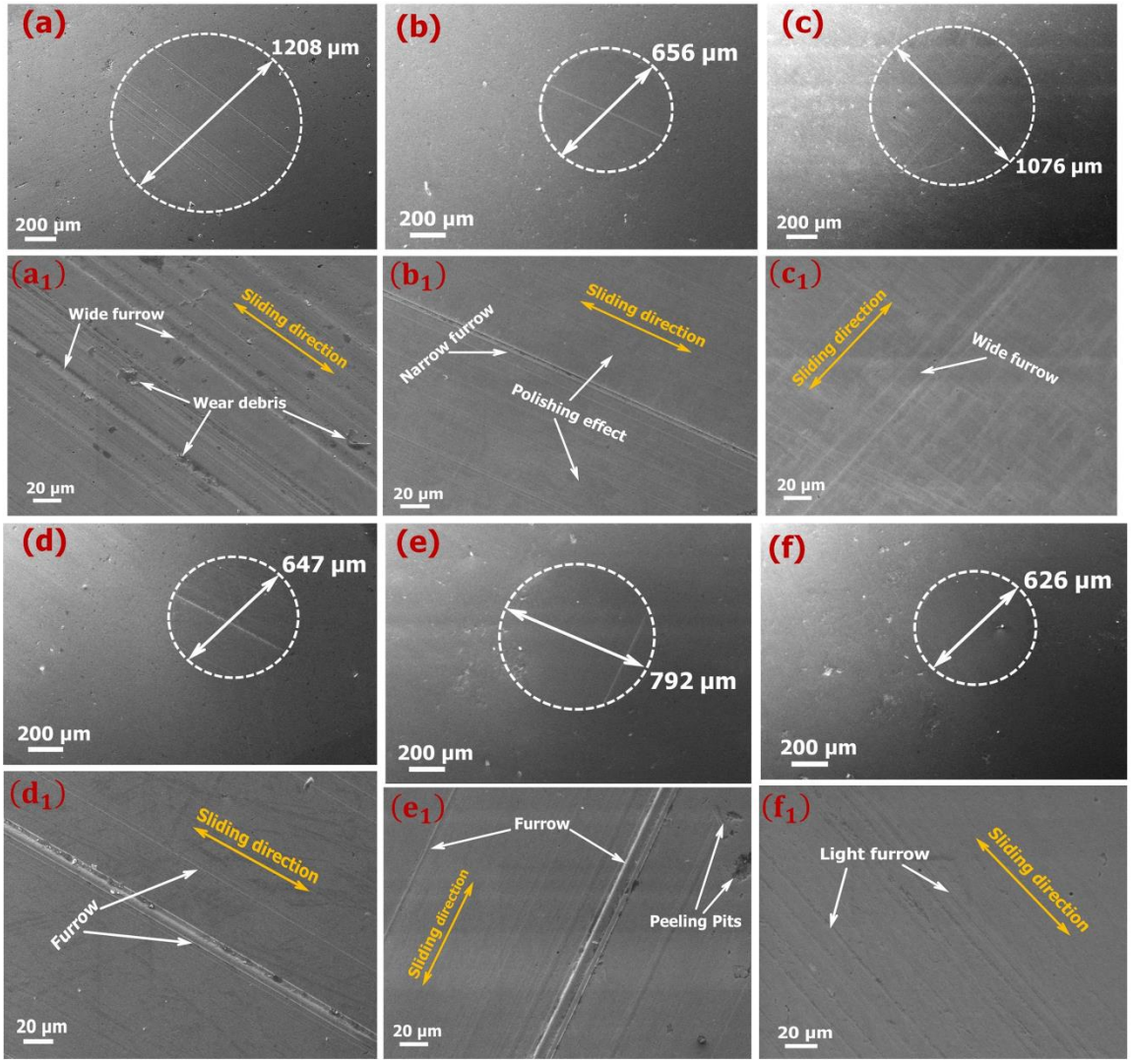

Figure 5.8: SEM micrographs of worn surfaces of steel ball tested with (a, a_1) pure PAO 4 at 50 N load and sliding velocity of 0.42 m/s; (b, b_1) PAO 4 with 0.075 wt.% MWCNTs at 80 N load and sliding velocity of 0.42 m/s; (c, c_1) pure PAO 6 at 80 N load and sliding velocity of 1.099 m/s; (d, d_1) PAO 6 with 0.05 wt.% MWCNTs at 80 N load and sliding velocity of 1.57 m/s; (e, e_1) pure PAO 40 at 100 N load and sliding velocity of 1.57 m/s; (f, f_1) PAO 40 with 0.075 wt.% MWCNTs at 50 N load and sliding velocity of 1.57 m/s

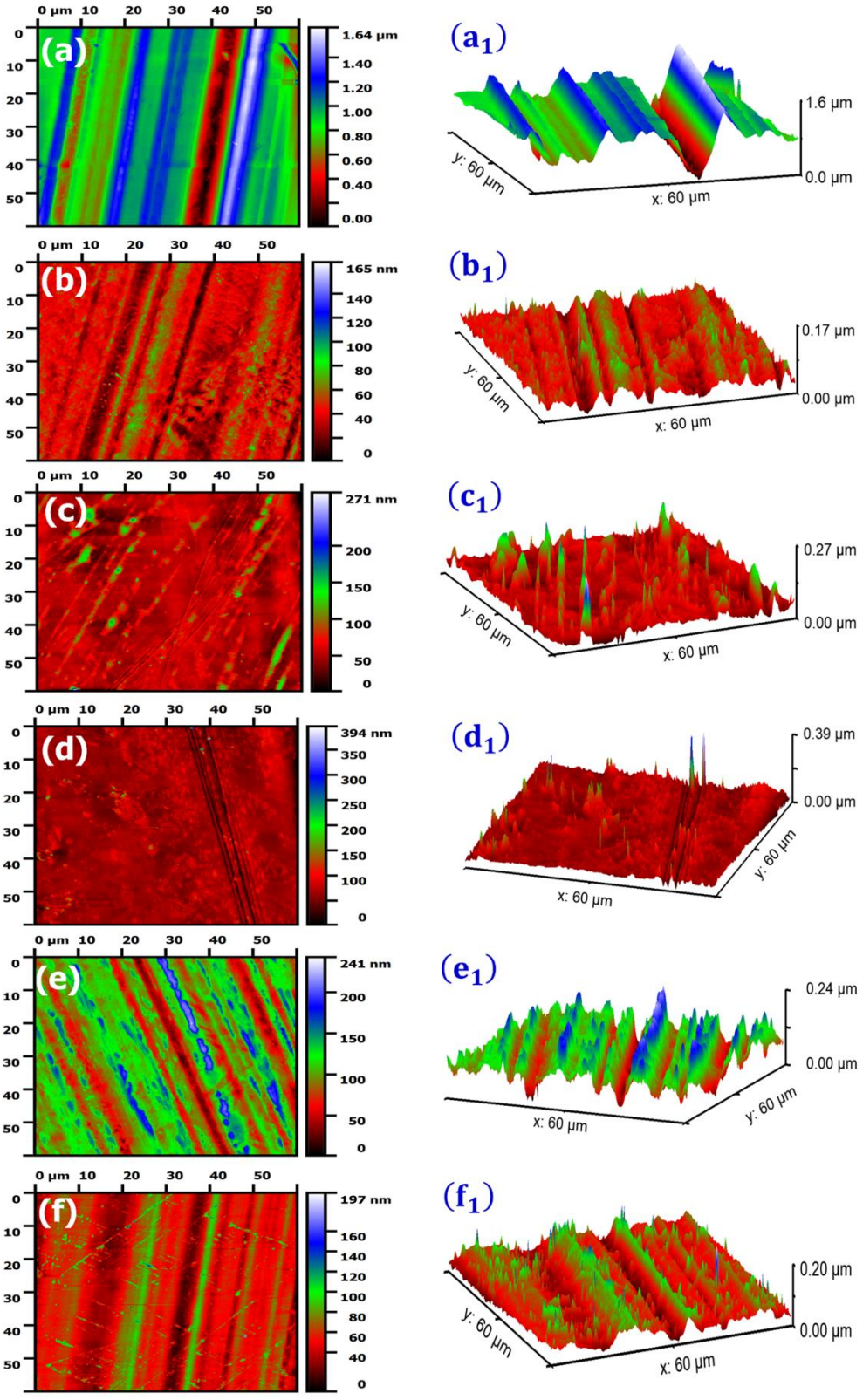

Figure 5.9: SPM images of worn surfaces of steel ball experimented with (a, a_1) pure PAO 4 at 50 N load and sliding velocity of 0.42 m/s; (b, b_1) PAO 4 with 0.075 wt.% MWCNTs at 80 N load and sliding velocity of 0.42 m/s; (c, c_1) pure PAO 6 at 80 N load and sliding velocity of 1.099 m/s; (d, d_1) PAO 6 with 0.05 wt.% MWCNTs at 80 N load and sliding velocity of 1.57 m/s; (e, e_1) pure PAO 40 at 100 N load and sliding velocity of 1.57 m/s; (f, f_1) PAO 40 with 0.075 wt.% MWCNTs at 50 N load and sliding velocity of 1.57 m/s

Table 5.9: The summary of surface roughness of worn steel balls test with various experimental conditions

Samples (Experiment no.)	Line roughness		Surface roughness	
	R_a (nm)	R_q (nm)	S_a (nm)	S_q (nm)
1	203	281	214.4	284.9
11	11.3	17.5	12.1	16.8
2	12.8	16.7	12.9	17.9
8	24.5	34.5	17.8	40.1
3	27.9	36.6	24.2	31.61
10	9.5	11.7	9.8	12.5

The EDS spectrum of the worn surfaces of steel balls tested at various experimental conditions is shown in **Figure 5.10**. The EDS spectra display the presence of Fe, C, Cr, and O for all worn surfaces. The existence of C on the worn surface may be due to the physical adsorption of MWCNTs during the friction process or maybe from the steel ball since the steel ball consists of iron, carbon, and chromium as a major ingredient. The presence of O manifests the formation of the oxide layer at the matting surface when the iron is exposed to air. It can be noticed that a higher weight % of carbon was observed on all worn surfaces lubricated with PAOs containing MWCNTs except worn surface tested with PAO 4 with 0.075wt% of MWCNTs. The comparison of worn surface tested with PAO 4 containing 0.075 wt.% of MWCNTs (**Figures 5.10(b)-5.10(b$_1$)**) with the worn surface lubricated with pure PAO 4 (**Figures 5.10(a)-5.10(a$_1$)**) which represents the higher weight % of carbon (19.1 wt.%), which is credited to the existence of wear residues on the surface. It is witnessed in SEM micrographs (**Figure 5.8(a)-5.8(a$_1$)**). The higher weight % of carbon illustrates that a lubricating oil film must have been developed and possibly comprised of

MWCNTs, which would have functioned as an intermediator to inhibit the direct metal-to-metal contact. Accordingly, the tribological properties were enhanced.

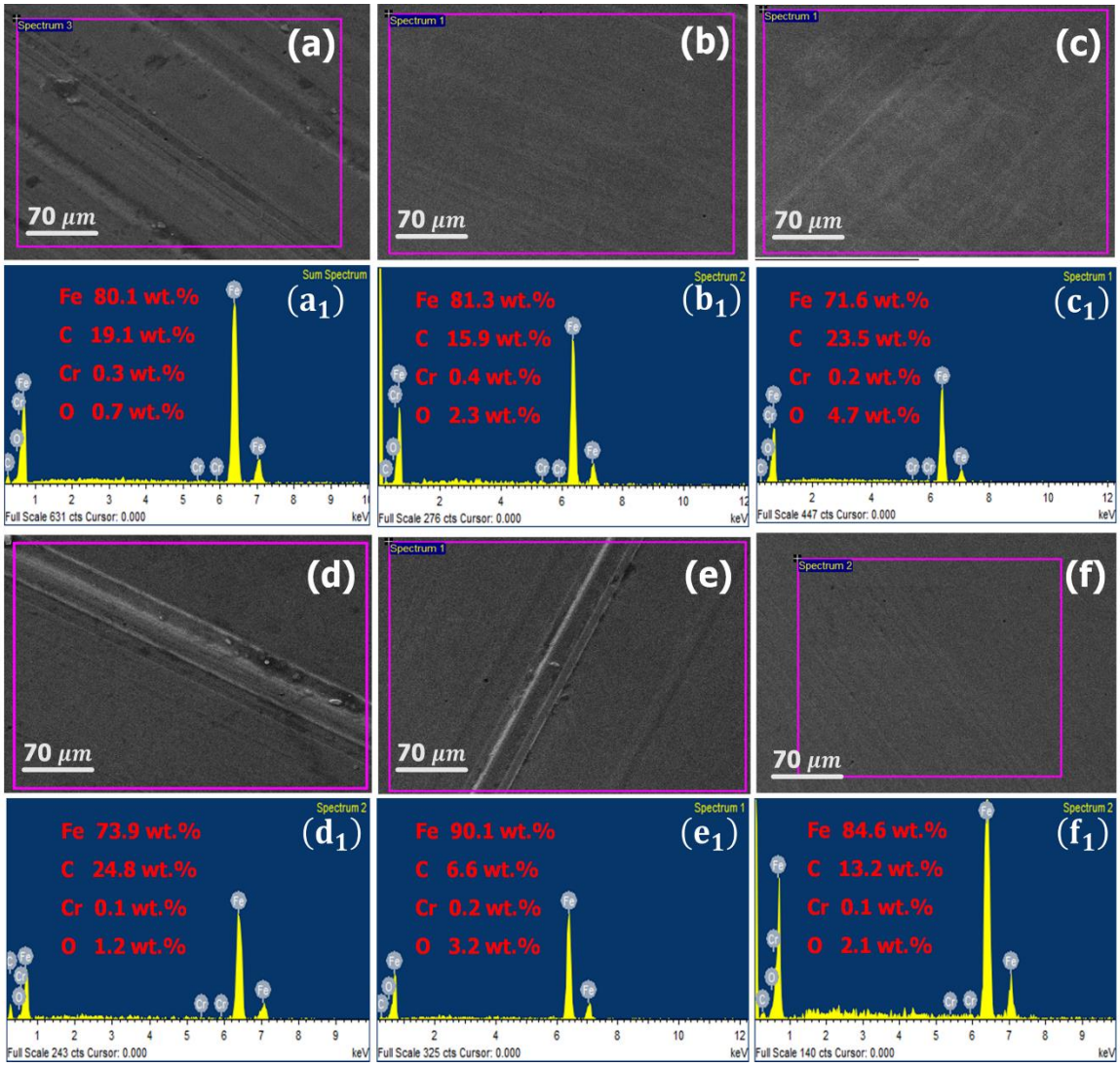

Figure 5.10: EDS spectra of wear scar of steel balls tested with (a, a_1) pure PAO 4 at 50 N load and sliding velocity of 0.42 m/s; (b, b_1) PAO 4 with 0.075 wt.% MWCNTs at 80 N load and sliding velocity of 0.42 m/s; (c, c_1) pure PAO 6 at 80 N load and sliding velocity of 1.099 m/s; (d, d_1) PAO 6 with 0.05 wt.% MWCNTs at 80 N load and sliding velocity of 1.57 m/s; (e, e_1) pure PAO 40 at 100 N load and sliding velocity of 1.57 m/s; (f, f_1) PAO 40 with 0.075 wt.% MWCNTs at 50 N load and sliding velocity of 1.57 m/s

5.6. Summary of the chapter

In this chapter, the concentration of COOH-functionalized multi-walled carbon nanotubes (MWCNTs), applied load, sliding velocity, and kinematic viscosity of polyalphaolefins (PAOs) were selected as process parameters or control factors. The coefficient of friction and specific wear rates (K) were considered the response factors (or output parameters). Taguchi's robust design method was used to analyse the influences of process parameters on the tribological performance of nanolubricants (i.e., response factors). The statistical results showed that the applied load, followed by a concentration of MWCNTs, conferred the most significant impact on the frictional characteristic. In contrast, the kinematic viscosity of PAOs, followed by the concentration of MWCNTs, has been observed as the most significant influencing factors on the anti-wear properties of nanolubricants.